Nitridation of one-dimensional tungsten oxide nanostructures: Changes in structure and photoactivity

Tamás Varga,[1] Henrik Haspel,[1,†] Attila Kormányos,[2] Csaba Janáky,[2,3] Ákos Kukovecz[1] and Zoltán Kónya[1,4*]

[1]Department of Applied and Environmental Chemistry, University of Szeged, H-6720 Szeged, Rerrich Béla tér 1, Hungary;

[2]Department of Physical Chemistry and Materials Science, University of Szeged, H-6720 Szeged, Rerrich Béla tér 1, Hungary;

[3]MTA-SZTE "Lendület" Photoelectrochemistry Research Group, H-6720 Szeged, Rerrich Béla tér 1, Hungary;

[4]MTA-SZTE Reaction Kinetics and Surface Chemistry Research Group, H-6720 Szeged, Rerrich Béla tér 1, Hungary;

*****Corresponding author: konya@chem.u-szeged.hu; Tel.: +36-62-544-620, Fax.: +36-62-544-619

†Present address: Division of Physical Sciences and Engineering, KAUST Catalysis Center (KCC), King Abdullah University of Science and Technology (KAUST), 4700 KAUST, Thuwal, 23955-6900, Saudi Arabia.

Highlights

- Tungsten oxide nanowires were transformed into nitrogen-doped nanostructures via high-temperature annealing in ammonia/nitrogen atmosphere.
- Tungsten oxide nanowires were first turned into tungsten oxynitride and then, at higher temperatures, into tungsten nitride nanosheets.
- Electronic band positions and corresponding bandgap were determined and compared to that of the nitrogen treated samples.
- Although the bandgap of tungsten oxide decreased as nitrogen incorporated into the structure, the corresponding photoactivity did not improve.

Abstract

In the search for stable, visible light active photoelectrodes, hydrothermally synthesized tungsten oxide nanowires were modified via nitrogen incorporation into their structure. To this end, nanowires were heat-treated in ammonia/nitrogen atmosphere at different temperatures. This procedure caused transitions in their structure that were investigated along with the photoelectrochemical properties of the samples. Results were subsequently compared to the reference samples treated in inert nitrogen atmosphere. Morphological changes and structural transitions were followed by transmission and scanning electron microscopy and X-ray diffraction. Bandgap energies were determined from the UV–vis spectra of the materials, while photoelectrochemical properties were tested by linear sweep photovoltammetry and electrochemical impedance spectroscopy. Pristine tungsten oxide nanowires were first

transformed into tungsten oxynitride and then tungsten nitride during high-temperature calcination in ammonia atmosphere. Electron microscopic investigation revealed that, along with phase transition, the initial fibrous morphology gradually converted into nanosheets. Simultaneously, bandgap energies significantly decreased in the calcination process, too. Photoelectrochemical measurements demonstrated that photoactivity in the treated samples was not improved by the decrease of the bandgap. This behavior might be explained with the deterioration of charge carrier transport properties of the materials due to the increased number of structural defects (acting as trap states), and current ongoing work aims to verify this notion.

Keywords: tungsten oxide, oxynitride, tungsten nitride, bandgap, photoelectrochemistry

1. Introduction

As a promising material, nanostructured tungsten oxide (WO_3), besides TiO_2, is one of the most investigated oxide semiconductors. Its high stability in acidic medium, accompanied by inherently attractive transport properties (hole diffusion length and electron Hall mobility is ~12 $cm^2\ V^{-1}\ s^{-1}$, compared to TiO_2 that is 0.3 $cm^2\ V^{-1}\ s^{-1}$),[1] make WO_3 suitable for a wide variety of possible applications in photovoltaics, photocatalysis, and gas sensing, etc.[2],[3],[4] Photoelectrochemical (PEC) properties of tungsten oxide nanostructures have been widely studied in the literature. Etched and reduced WO_3 nanoflakes showed increased photocurrent density (1.10 mA cm^{-2} at 1.0 V vs Ag/AgCl) compared to the pristine WO_3 (0.62 mA cm^{-2}), which was assigned to the formation of oxygen vacancies on a rough surface. [5] Su et al. prepared tungsten oxide films containing nanowire arrays. The highest photocurrent topped 1.43 mA cm^{-2} using an irradiation source emitting at the edge of the visible light (400 nm). [6] Hydrogen treatment of tungsten oxide can also soar the photoactivity by an order of magnitude of the pristine WO_3, along with the improvement in the photostability of the structure.[7]

These materials possess a relatively wide bandgap (2.5–2.8 eV), implying that only the higher-energy region of the solar spectrum (UV and the higher energy visible part, i.e., blue/violet light) can be utilized in the photogeneration of electron–hole pairs. To widen the restricted absorption range, the bandgap energy can be modified by, for example doping with various transition metals, nitrogen, sulfur or carbon.[8],[9],[10],[11] The latter modifications are accompanied by the variation in the electrochemical properties as well. A review by Janáky dealt with the change of band structure and photocatalytic activity after doping WO_3 with different type of elements.[12] Liu et al. investigated nitrogen-doped graphene and reached a

1.8-fold increase in the photoactivity compared to the pure nanoporous WO_3 photoelectrode.[13]

PEC performance of pristine WO_3 can be further enhanced by nitridation (i.e., nitrogen doping or alloying). A recent review by Domen discussed the bandgap narrowing with the substitution of oxygen with nitrogen.[14] As **Fig. 1** demonstrates, the N 2p orbital can form a filled energy state above the O 2p state. These types of tungsten oxynitrides and nitrides are generally more stable than other known non-oxide semiconductors.[14]

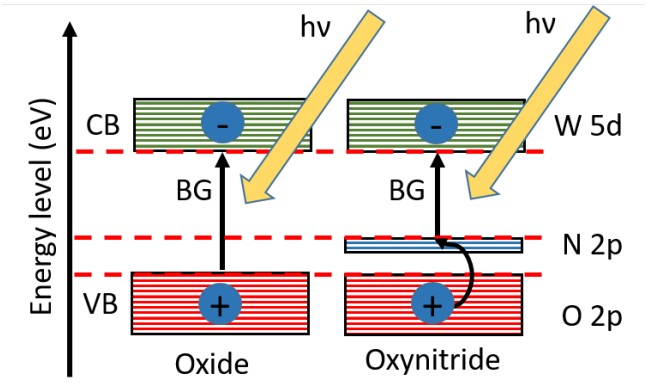

Fig. 1. Narrowing the bandgap (BG) during nitrogen incorporation into the oxide structure.

There are several ways to realize nitrogen-doped tungsten oxide or tungsten nitride nanostructures; for instance, depositing nitrogen-doped WO_3 thin films employing reactive magnetron sputtering in nitrogen atmosphere,[15] or synthesizing tungsten nitride nanorods via a hydrothermal method using tungstic acid and ammonium sulfate.[16] The simple thermal treatment is a straightforward method to synthesize mesostructured tungsten nitride with the calcination of tungstic acid powder in ammonia atmosphere at 700 °C or nanoporous layers in ammonia atmosphere up to 600 °C.[17] The nitrogen content as well as the PEC properties are influenced by the annealing time. In certain instances, the photocurrent becomes 18-times higher than that of the pure WO_3, however, high-temperature annealing (~600 °C or above) decreases the photoresponse because of the degradation of the crystalline structure.[18] Nanoporous WO_3 photoelectrodes were heat-treated in NH_3/N_2 atmosphere with different compositions at 450 °C and the highest photocurrent density was attained in 1:2 NH_3:N_2 mixture.[13] The suggested mechanism of the annealing process is as follows. Ammonia decomposes at high temperature, and the resulting nascent nitrogen helps in creating a specific

atmosphere inside the furnace that reacts with the sample to form nitrogen doped/alloyed tungsten oxide or tungsten nitride.[17],[19]

Here, we report the ammonia treatment of hydrothermally synthesized tungsten oxide nanowires in 1:2 NH_3:N_2 atmosphere at different annealing temperatures. The morphological, structural, and photoelectrochemical changes were followed along with the incorporation of nitrogen into the structure. Results are discussed in comparison to the samples treated in inert nitrogen atmosphere. Most importantly, the bandgap narrowing was not mirrored by the alteration in the PEC properties, highlighting the importance of other structural factors—beyond light absorption—that dictates photoactivity.

2. Experimental

2.1. Synthesis of tungsten oxide nanowires

Tungsten oxide nanowires were synthesized via a hydrothermal route. First, 3.56 g sodium tungstate dihydrate ($Na_2WO_4 \cdot 2H_2O$, Sigma Aldrich) and 4.28 g sodium sulfate decahydrate ($Na_2SO_4 \cdot 10H_2O$, Sigma Aldrich) were dissolved in 115 cm^3 deionized water. Then, the pH of the solution was adjusted to 1.5 via adding nitric acid (3 $mol \cdot dm^{-3}$) dropwise to the clear continuously stirred solution. After 30 min stirring, the solution was transferred into a Teflon-lined stainless steel autoclave and heat treated at 180 °C for 24 hours. Finally, the product was obtained by membrane filtration, washed with deionized water, and then dried at 80 °C overnight.

2.2. Preparation of ammonia-treated tungsten oxide nanowires

Nanowires were heat treated in 1:2 ammonia/nitrogen atmosphere with a flow rate of 120 $cm^3\ s^{-1}$ at different temperatures. On the contrary, the reference samples were heat treated only in pure nitrogen atmosphere.

2.3. Morphological and Structural Characterization

Morphological changes of the samples were investigated by transmission and scanning electron microscopy techniques (TEM, SEM), using an FEI Tecnai G^2 20 X Twin microscope at 200 kV accelerating voltage and a Hitachi S4700 Field Emission SEM, respectively. For SEM studies, the samples were spread on a carbon tape surface, which was attached to an aluminum sample holder, while TEM samples were sonicated in isopropyl alcohol before being dropped on a copper mounted holey carbon film and dried subsequently. The crystal structure of the samples was analyzed by phase identification via X-ray diffraction (XRD) using Cu Kα

radiation (k = 1.5406 Å) in a Rigaku Miniflex II instrument. The X-ray photoelectron spectra (XPS) were collected with a SPECS instrument using a PHOIBOS 150 MCD 9 hemispherical electron energy analyzer, using the Kα radiation of the Al anode ($h\nu$ = 1486.6 eV). The X-ray gun was operated at 210 W (14 kV, 15 mA), and the analyzer in FAT mode, with 20 eV pass energy. Five scans were averaged to obtain a single high-resolution spectrum. The binding energy scale was corrected by the deconvolution of the complex C 1s region as the carbon peak was fixed at 285.1 eV. Raman spectra of the samples were measured at 532 nm laser excitation energy with 5 mW power using a Thermo Scientific DXR Raman Microscope. Typically, ten scans were recorded and averaged with 1 cm^{-1} resolution in the 200–3500 cm^{-1} range. Diffuse reflectance UV–vis spectroscopy was used to investigate the bandgap energy of the catalysts with fiber optic system consisting of a Micropack HPX-2000 light source and an Ocean Optics USB2000 detector. The detector has 2048 pixel resolution in the 200–1100 nm wavelength range.

2.4. Photoelectrochemical measurements

2.4.1. Preparation of photoelectrodes for photoelectrochemical measurements

All samples were dispersed in isopropanol (c = 5 mg cm^{-3}) by ultrasonic treatment for 30 min before deposition. The samples were spray-coated on a preheated (140 °C) glassy carbon electrode surface, using an Alder AD320 type airbrush and a homemade spray-coater robot, operated with 1 bar compressed air. The loading of the materials on the electrode surface was approximately 0.1 mg. After the spray-coating step, the resulted thin layers were heat treated in an oven at 180 °C for 60 min. This annealing had a dual purpose: i) to remove any residual traces of the solvent, and ii) to enhance the adhesion of the spray-coated layers to the underlying electrode surface.

2.4.2. Photovoltammetry and Mott–Schottky analysis

All PEC measurements were performed using a Metrohm Autolab PGSTAT302 type potentiostat/galvanostat in a sealed, custom-designed, one-compartment, three-electrode quartz cell. Glassy carbon electrodes, that are modified with various tungsten oxide samples, were used as working electrode, while a Pt sheet and Ag/AgCl/3 M NaCl were employed as counter and reference electrodes, respectively. The light source was a 300 W Hg–Xe arc discharge lamp (Hamamatsu L10852). The spectrum of the light source is presented in the Supplementary Data (**Fig. S10**). The radiation source was placed 5 cm away from the illuminated working electrode surface and shone through a quartz window. The output power, reaching the working electrode surface was 180 mW cm^{-2} in this configuration. The frequency of the chopped illumination was

set to 0.1 Hz, while the applied sweep rate was maintained at 2 mV s^{-1}. Sulfuric acid (H_2SO_4, Molar, 0.5 mol·dm^{-3}) was used as electrolyte solution, saturated by Ar for 30 minutes before each measurement. For Mott–Schottky analysis, the electrochemical impedance spectra of the electrodes were recorded at 13 different potentials (E = −0.6 V–0.1 V vs. Ag/AgCl/3 M NaCl) in 0.5 M sulfuric acid solution, between 10 Hz and 10 kHz frequency, using sinusoidal excitation signal with 10 mV RMS amplitude in the absence of illumination. The Mott–Schottky plots were generated by using the NOVA software of the Autolab instrument. Results, that were collected at 1500 Hz frequency, are presented in this study.

3. Results and discussion

3.1. Morphology

Morphological changes of WO_3 nanowires, thermally treated in NH_3/N_2 atmosphere, were monitored by TEM (**Fig. 2)**. **Fig. 2a** shows the as prepared tungsten oxide nanowires with ~1–2 µm length and 100–150 nm diameter. There were no changes in the fibrous structure below 400 °C – only smaller pieces peeled off the nanowires, as seen in the inset of **Fig. 2c.** These one-dimensional structures started to break into smaller particles at 500 °C, while two-dimensional structures formed at 700 and 800 °C with typical side lengths of a few hundred nanometers (**Fig. 2f–g)**. **Fig. S1** demonstrates the TEM images of the reference samples thermally annealed in N_2 atmosphere. These nanowires are even more fragmented after calcination at high temperatures than the ammonia-treated ones. SEM images displayed similar morphology changes (**Fig. S2)**.

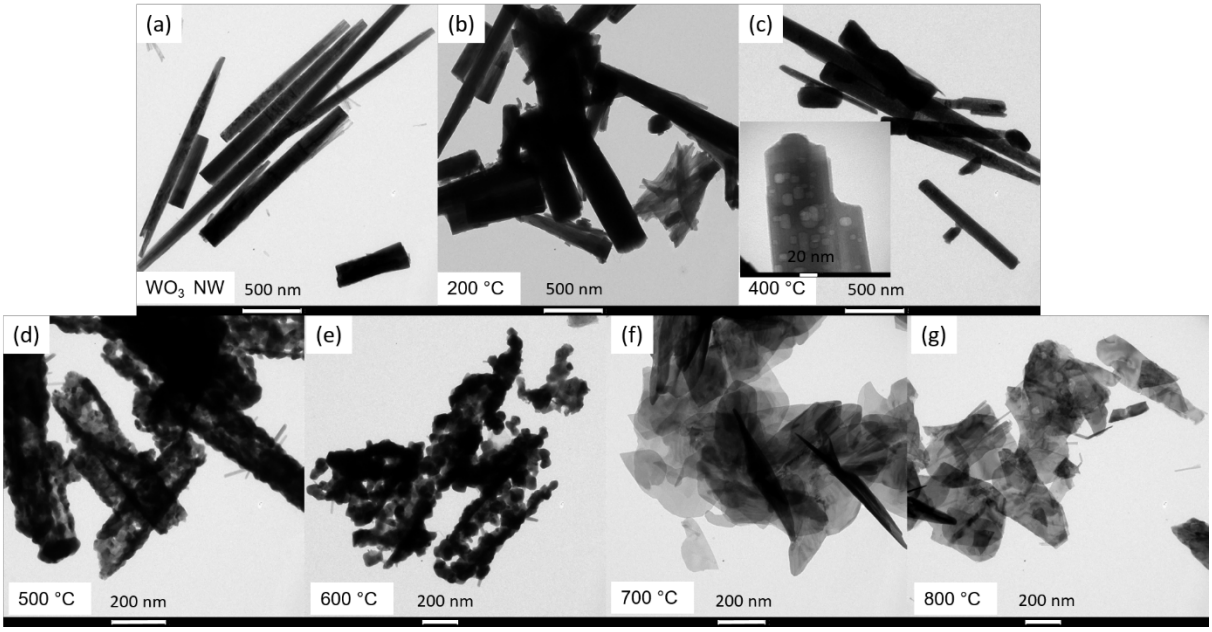

Fig. 2. TEM images of WO_3 nanowires (a) and nanowires treated in NH_3/N_2 atmosphere at 200 °C (b), 400 °C (c), 500 °C (d), 600 °C (e), 700 °C (f), and 800 °C (g).

Fig. 3 shows SEM images of pristine nanowires and nanowires treated in NH_3/N_2 atmosphere at different temperatures. The fibrous structure did not change below 400 °C. According to **Fig. 3d–e**, there is a mixture of nanowires and smaller particles at 500 °C, while nanolayers and smaller particles dominate the sample at 600 °C. Thermal annealing at and above 700 and 800 °C transformed the nanowires into two-dimensional nanolayers (**Fig. 3f-g)**.

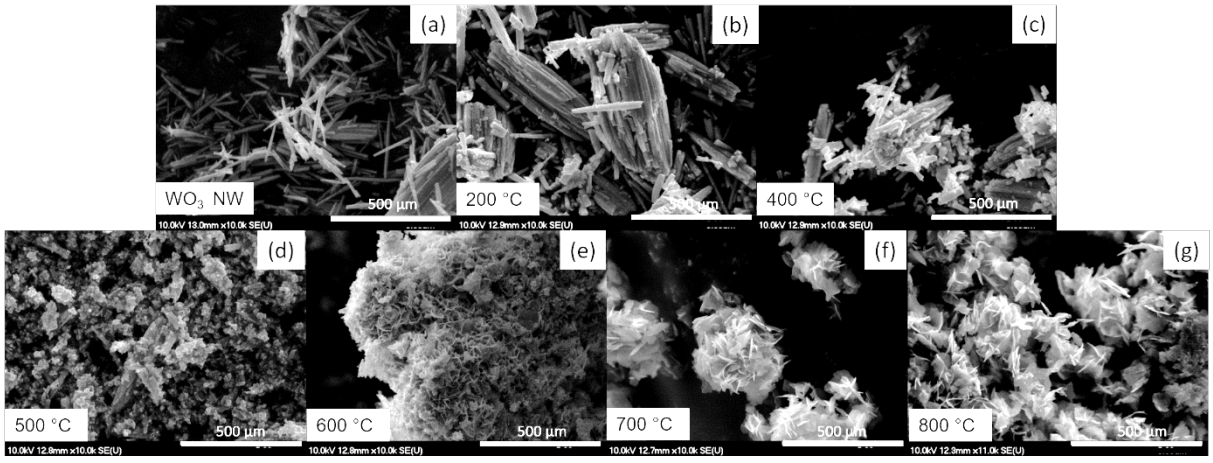

Fig. 3. SEM images of WO_3 nanowires (a) and nanowires treated in NH_3/N_2 atmosphere at 200 °C (b), 400 °C (c), 500 °C (d) 600 °C (e), 700 °C (f), and 800 °C (g).

3.2. Structure and composition

The structural changes of the nanowires were monitored by XRD as well (**Fig. 4).** During annealing in NH_3/N_2 atmosphere at 400 °C, hexagonal WO_3 (h-WO_3) (JCPDS 00-033-1387) started to transform into monoclinic WO_3 structure (m-WO_3) (JCPDS 01-072-1465) and then turned into tungsten oxynitride and tungsten nitride at even higher temperatures (Fig. **4 a–b**,). There is a mixture of $H_{0.33}WO_3$ [20] (JCPDS 00-006-0706) and $W_{0.62}(N_{0.62},O_{0.38})$ at 500 °C, and $W_{0.62}(N_{0.62}O_{0.38})$ and W_2N_3 at 600 °C [21] (JCPDS 00-025-1254) at 600 °C, respectively. The hexagonal nanowires, however, were still present in the sample at 600 °C. Annealing at and above 700 °C transformed the structure into W_2N_3.[22] The heat treatment in nitrogen atmosphere also started to transform the hexagonal structure (h-WO_3) (JCPDS 00-033-1387) of the nanowires into monoclinic at 400 °C. A mixture of hexagonal and monoclinic phases composed the sample between 400 and 700 °C, while only the monoclinic structure (m-WO_3) and its reflections were discernible at 700 °C and above. Szilágyi et al. investigated the thermal stability of hexagonal tungsten oxide in air, and they found that the structure collapsed at 550–600 °C and irreversibly transformed into monoclinic structure. Our findings are in good agreement with these literature results.[23]

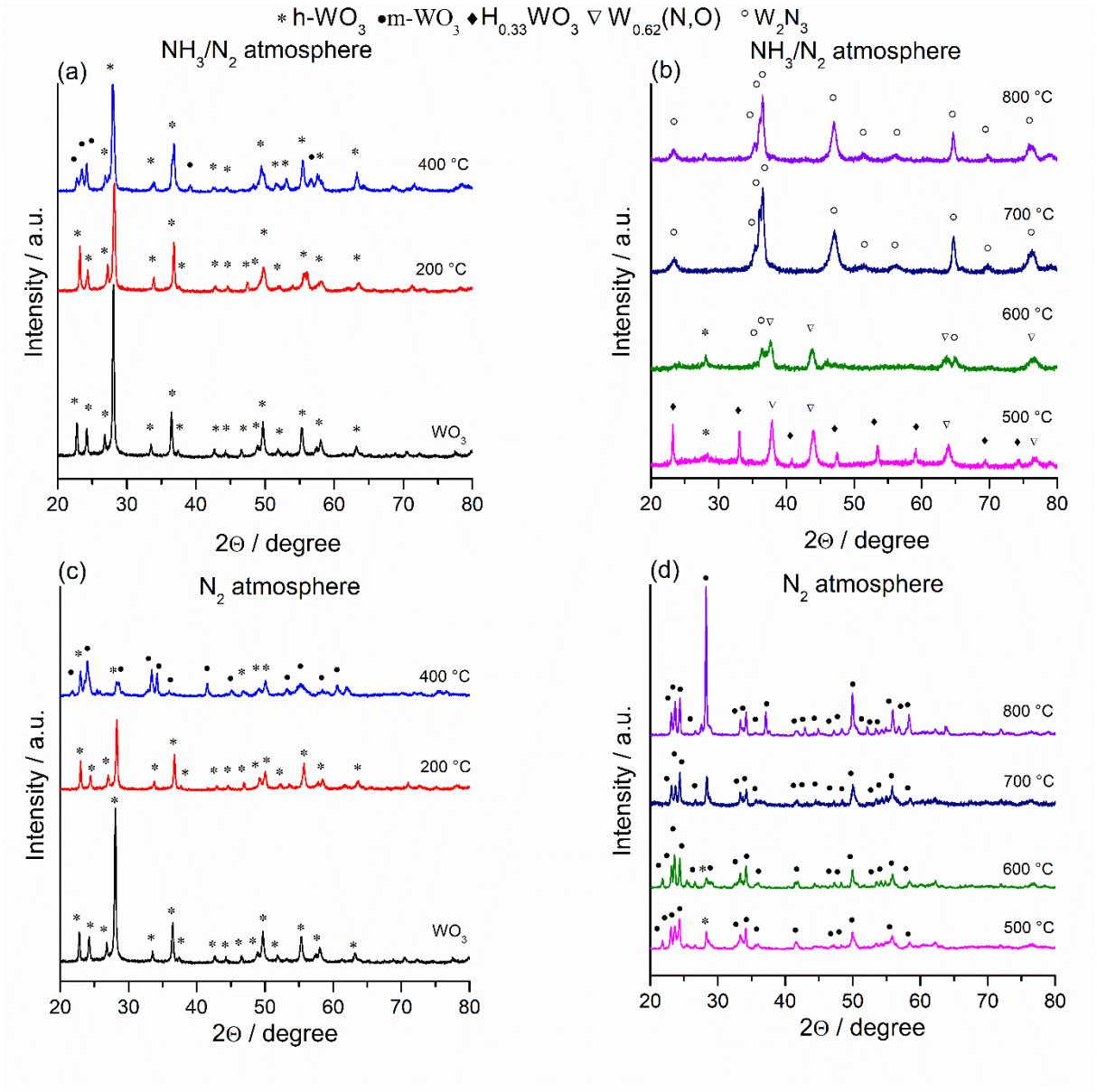

Fig. 4. XRD patterns of WO_3 nanowires heat treated in NH_3/N_2 atmosphere at (a) 200–400 °C and (b) 500–800°C; and in N_2 atmosphere at (c) 200–400 °C and (d) 500–800 °C.

Fig. 5a shows the Raman spectra of WO_3 nanowires after the heat treatment in NH_3/N_2 atmosphere. The well-defined bands of WO_3 at 967, 812, 756, 665, 328, and 239 cm^{-1} correspond to the hexagonal phase of tungsten oxide.[24] The peaks at 967 and 928 cm^{-1} were attributed to the stretching mode of the –W=O terminal modes and the stretching mode of WO_2. These two peaks merged at higher temperature, and a further band emerged at 946 cm^{-1}. This corresponds to the stretching vibration of O–W–O, whose intensity decreases at and above 700 °C. The position of the band at 812 cm^{-1} – also a stretching O–W–O band – shifted to lower wavenumbers at lower annealing temperatures, due to oxygen loss from the WO_3 structure. Treatment at higher temperatures shifted the band back toward higher wavenumbers, as a result

of the phase transformation from hexagonal into monoclinic WO_3 structure.[25],[26] The stretching modes of the transition metal bonds at 756 cm^{-1}, and the out of plane wagging mode of O–W–O at 665 cm^{-1} are also merged at 400 °C and shifted to lower wavenumbers. The band position of the bending vibrations of O–W–O at 328 cm^{-1} is also red shifted at lower treatment temperatures and regained during the annealing at higher temperatures. Raman spectra of the samples, treated at 700 and 800 °C showed predominant bands at 805, 680, and 250 cm^{-1}, which correspond to the tungsten nitride phase.[26]

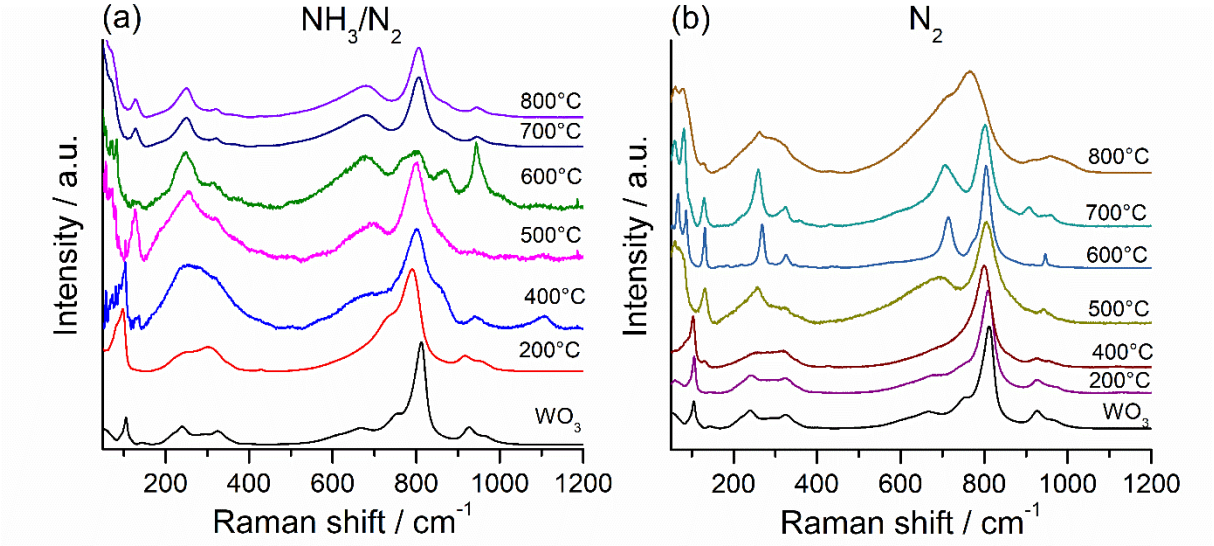

Fig. 5. Raman spectra of WO_3 nanowires annealed in (a) NH_3/N_2 and (b) N_2 atmosphere at the temperatures indicated in the figure.

Changes in the Raman spectra after heat treatment in nitrogen atmosphere are shown in **Fig. 5b**. The changes of the bands at 812, 756, and 665 cm^{-1} are marks of the phase transformation of tungsten oxide from hexagonal to monoclinic phase. While three bands correspond to the hexagonal structure, only two bands represent the monoclinic one. The band at 812 cm^{-1} shifted to lower wavenumbers during heat treatment up to 400 °C, again due to the oxygen loss from WO_3. It regained its original position as the phase transformation from hexagonal to monoclinic WO_3 structure took place at higher temperatures.[25] The band at 239 cm^{-1} also shifted during the thermal treatment. Furthermore, there are three new bands at 67, 89, and 126 cm^{-1} at and above 500 °C treatment temperature. These peaks correspond to low-frequency phonon modes, known as temperature change markers. Similar bands are observed in the samples treated in NH_3/N_2 atmosphere, too.[27]

Fig. 6 shows the W4f XPS data of the ammonia-treated WO_3 nanowires (additional spectra measured for the other samples are presented in the supplementary data). The spin orbital

positions of 4f electrons for tungsten were observed at binding energies corresponding to 35.7 eV and 37.8 eV, which can be assigned to the +6 oxidation state.[28]

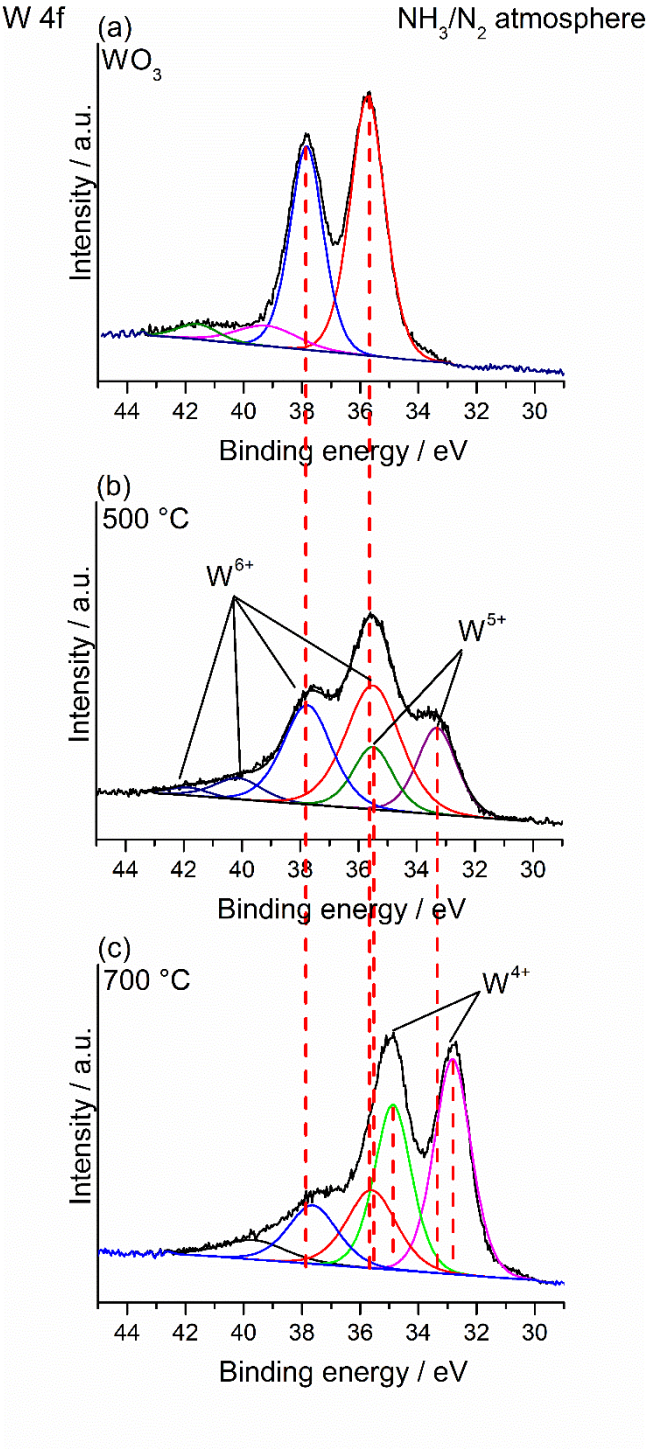

Fig. 6. W 4f X-ray photoelectron spectra of WO_3 nanowires (a) and nanowires treated in NH_3/N_2 atmosphere at 500 (b) and 700 °C (c).

New peaks appeared after heat treatment at 500 °C, and over 600 °C. The peak positions at 33.3 eV and 35.5 eV correspond to the binding energies of W^{5+}. The two peaks at 32.7 eV and 34.8

eV are attributed to the +4 oxidation state of tungsten in the nitride structure.[29],[30] The intensity of these two peaks increased, while the characteristic peaks of W^{6+} had lower intensity with increasing annealing temperature. **Fig. S3a** shows the nitrogen 1s XP spectra. The characteristic peak at 397.3 eV can be assigned to N 1s of W-N.[31] **Fig. S3b** shows the XPS spectra of oxygen and demonstrates that the peak intensity is lower at higher temperatures.

Further quantitative analysis was carried out to determine the approximate ratio of tungsten, oxygen, and nitrogen in the samples. The normalized area under the individual XPS peaks for tungsten, oxygen, and nitrogen were divided by their corresponding sensitivity factor and their ratio has been calculated and summarized in **Table S1.** The atomic percentage of oxygen decreased at higher temperatures from 73% to 33%, and nitrogen content increased up to 27% above 500 °C. The oxygen content can be partly ascribed to the presence of the adsorbed oxygen contained functional groups on the surface. **Fig S5** shows the W 4f XPS spectra of the samples treated in nitrogen atmosphere, and the characteristic peaks of the +6 oxidation state at 35.7 eV and 37.8 eV were observed in every sample.

The bandgap energies of the samples were calculated from UV–vis diffuse reflectance spectra using the Kubelka–Munk and Tauc equation. Tauc plots are shown in **Fig. S6**, while the results are summarized in **Fig. S6d**. The bandgap of the WO_3 nanowires narrowed from 3.3 to 2.7 eV due to annealing in N_2 atmosphere along with the transformation of the hexagonal structure to monoclinic. In the case of NH_3/N_2 atmosphere, the bandgap decreased further to 2.5 eV. Above 500 °C, it cannot be accurately determined because the black color of the samples hinders data recording. Nevertheless, we expect that the bandgap narrowed further during higher temperature annealing, as a result of the intermixing of N 2p states the above O 2p states.[32],[14]

3.3. Photoelectrochemical properties

The PEC behavior of the spray-coated samples was characterized by linear sweep photovoltammetry. According to the results, gleaned from the DRS UV–vis spectra, the smaller bandgap of the ammonia-treated WO_3 samples (especially the ones, heat treated above 400 °C) allows the excitation of these materials with visible light. Thus, as the first step, PEC measurements were carried out using solar irradiation. Surprisingly, only marginal photocurrents were measured (data not shown), indicating that the narrow bandgap is a necessary, but not a sufficient factor for visible light photoactivity (see discussion below). Better results were obtained employing UV–vis irradiation (**Fig. 7.).**

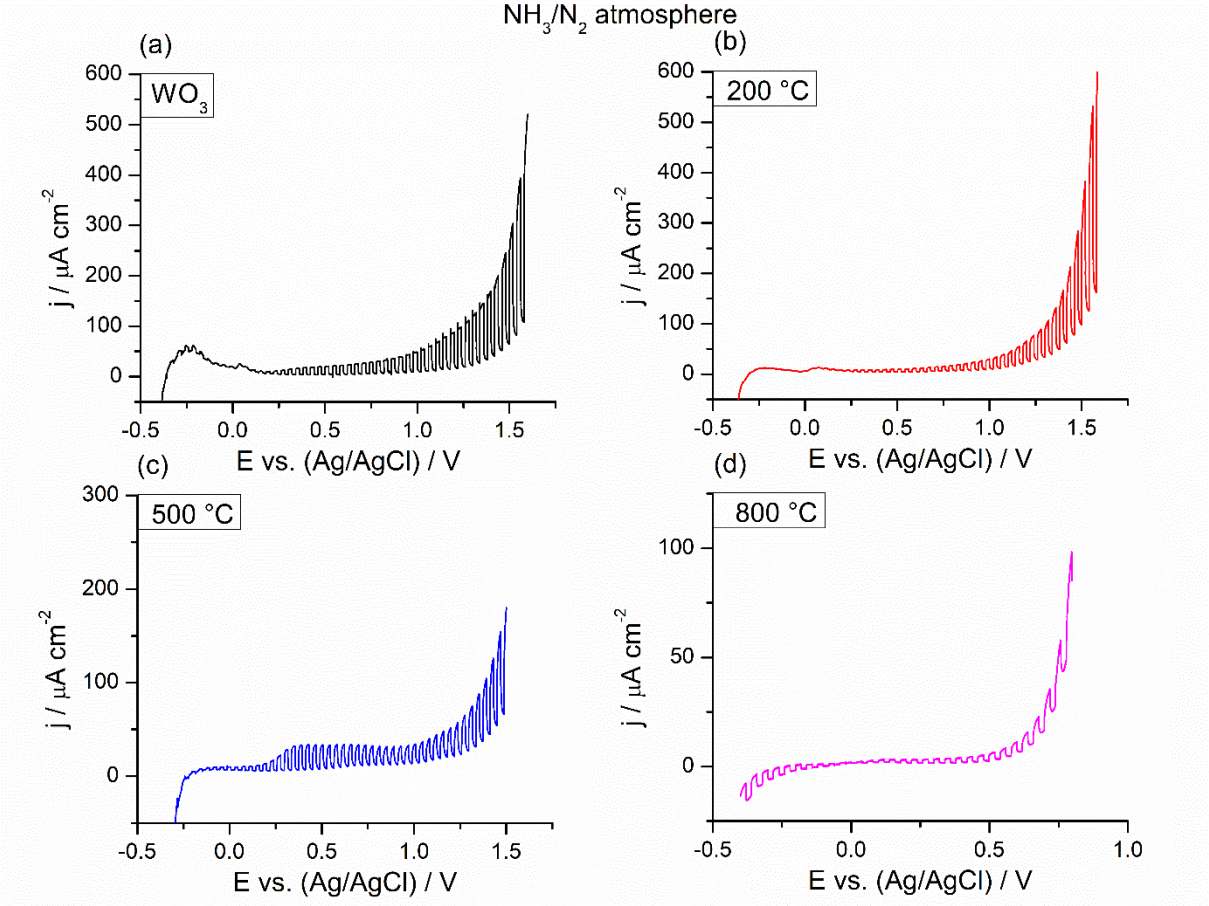

Fig. 7. Linear sweep photovoltammograms recorded for WO_3 samples heat treated in $NH_3//N_2$ atmosphere at various temperatures. A 300 W Hg–Xe lamp was used as a light source with a chopping frequency of 0.1 Hz. Measurements were performed in 0.5 M H_2SO_4 solution applying 2 mV s^{-1} sweep rate.

An n-type behavior was seen for all samples with anodic photocurrents. The recorded photocurrents, however, were not very impressive compared to earlier studies on nanoporous WO_3 films.[33],[34] The harvested photocurrents were not improved significantly by varying the film thickness (data not shown). Furthermore, photocurrents are decreasing together with the potential window, where the given material is photoactive, with the increasing temperature of the heat treatment procedure. Specifically, the onset potential of the photocurrents gradually shifted to more positive potentials. Taken together all these observations as a whole we can conclude that by introducing nitrogen atoms to the WO_3 crystal structure the bandgap gradually decreases, but this effect is accompanied by the formation of traps (i.e., charge carrier recombination centers). These traps hinder the transport of the photogenerated charge carriers toward both the solution and to the supporting electrode surface, resulting in small photocurrents.

XRD data suggested that when WO_3 was heat treated in nitrogen atmosphere, it has only changed its crystal structure from the hexagonal to the monoclinic polytype. This observation was also reflected on their photovoltammograms (only two sets are presented in **Fig. 8**, the others are shown in the supplementary data). Similarly to the previously presented results, an n-type behavior was seen. The maximum values of the photocurrent are in the same regime (100–150 µA cm^{-2}). Only the sample heat treated at 700 °C stands out: in this case higher photocurrents developed at less positive potentials compared to the others.

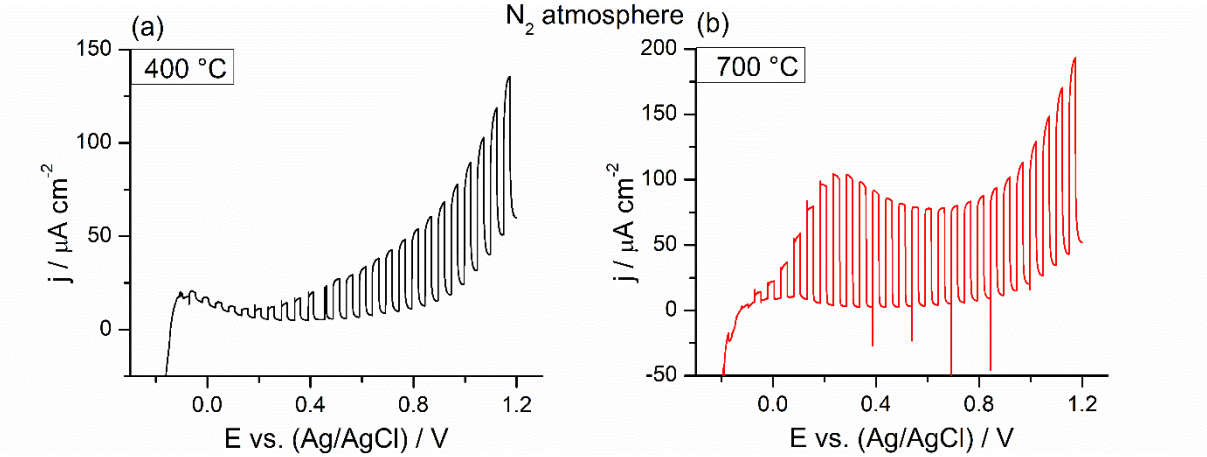

Fig. 8. Linear sweep photovoltammograms recorded for WO_3 samples heat treated in N_2 atmosphere at various temperatures. A 300 W Hg-Xe lamp was used as a light source with a chopping frequency of 0.1 Hz. Measurements were performed in 0.5 M H_2SO_4 solution applying 2 mV s^{-1} sweep rate.

Photocurrents, measured during the linear sweep voltammetry experiments were too small to confidently determine the flatband potential for all samples. In this vein, Mott–Schottky plots were recorded from EIS measurements (**Fig. 9, see also Fig. S9 for two representative Nyquist plots)**. The positive slopes confirmed the previously seen n-type behavior, while the measured C^{-2} values are comparable to the data found in the literature.[7],[13] **Fig. 9a** shows the plots recorded for the WO_3 samples, treated in ammonia atmosphere.

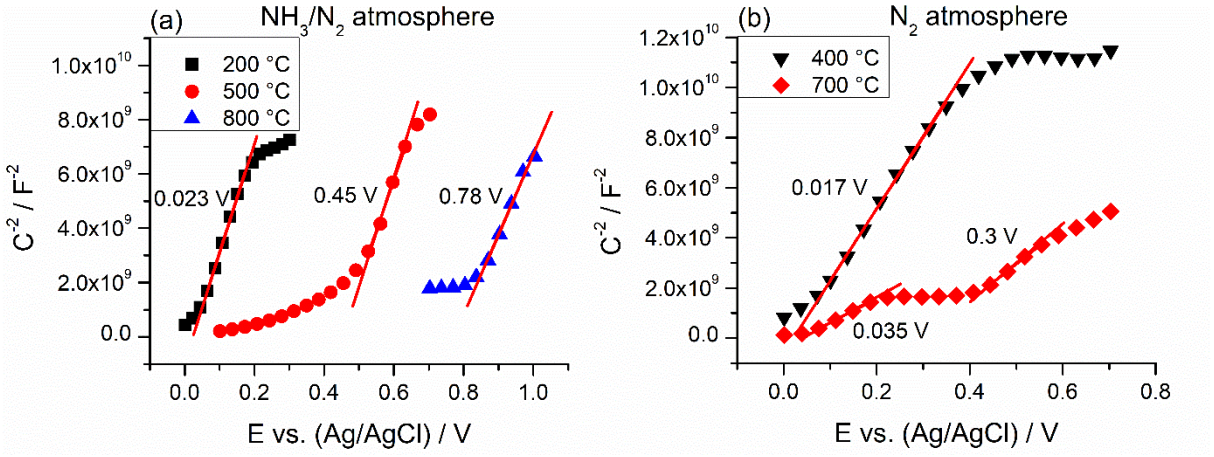

Fig. 9. Mott–Schottky plots, recorded for (a) WO_3 samples heat treated in NH_3 atmosphere at various temperatures, and (b) WO_3 samples heat treated in N_2 atmosphere at various temperatures. Measurements were performed in 0.5 M H_2SO_4 saturated with Ar.

By increasing the calcination temperature, the flatband potential (corresponding to the conduction band of these n-type semiconductors[35]) shifted toward more positive potential values (in agreement with the photovoltammetry data shown earlier). Interestingly, a different phenomenon was observed for the WO_3 samples heat treated in nitrogen atmosphere: two linear sections can be identified, and thus two flatband potentials were calculated for the sample heat treated at 700 °C. The first one is similar to the one, calculated for the WO_3 sample, heat treated at 400 °C, attributed to the hexagonal polytype of WO_3. The appearance of the second flat-band potential is an unexpected phenomenon because according to the XRD data, only monoclinic WO_3 is supposed to be present in this sample.

4. Conclusions

In summary, hydrothermally synthesized tungsten oxide nanowires were thermally treated in ammonia/nitrogen atmosphere at different temperatures. The morphology of the nanowires was turned into cracked nanowires and nanosheets accompanied by the structural transformation of the hexagonal phase into monoclinic WO_3, and tungsten oxynitride and nitride at higher annealing temperatures. Although incorporation of nitrogen atom narrowed the bandgap of the pristine nanowires, photovoltammetric measurements demonstrated the lack of improvement in photoactivity. As a possible, yet not fully proven, explanation, we think that trap states, formed in the material during N-incorporation, hinder the transport of the photogenerated charge carriers toward both the solution and the supporting electrode surface. These results confirm that while N-incorporation is a viable strategy to narrow the bandgap of WO_3, other structural factors need to be also considered to achieve enhanced PEC behavior.

Further mechanistic studies, focusing on the charge carrier recombination dynamics, are in progress in our laboratories.

Acknowledgements

The financial support of the Hungarian Research Development and Innovation Office through grants NKFIH OTKA K 112531 (Á.K.), K 120115 (Z.K.) and GINOP-2.3.2-15-2016-0013 (Cs. J., Á.K., Z.K.) is acknowledged. The authors are grateful to Dr. Albert Oszkó (University of Szeged) for recording XPS spectra.

Appendix A. Supplementary data

References

[1] Q. Mi, A. Zhanaidarova, B.S. Brunschwig, H.B. Gray, N.S. Lewis, A quantitative assessment of the competition between water and anion oxidation at WO3 photoanodes in acidic aqueous electrolytes, Energy & Environmental Science, 5 (2012) 5694–5700.

[2] T. He, J. Yao, Photochromic materials based on tungsten oxide, Journal of Materials Chemistry, 17 (2007) 4547–4557.

[3] Y. Liu, Y. Ohko, R. Zhang, Y. Yang, Z. Zhang, Degradation of malachite green on Pd/WO3 photocatalysts under simulated solar light, Journal of hazardous materials, 184 (2010) 386–391.

[4] X. An, J.C. Yu, Y. Wang, Y. Hu, X. Yu, G. Zhang, WO3 nanorods/graphene nanocomposites for high-efficiency visible-light-driven photocatalysis and NO2 gas sensing, Journal of Materials Chemistry, 22 (2012) 8525–8531.

[5] W. Li, P. Da, Y. Zhang, Y. Wang, X. Lin, X. Gong, G. Zheng, WO3 Nanoflakes for Enhanced Photoelectrochemical Conversion, ACS Nano, 8 (2014) 11770–11777.

[6] J. Su, X. Feng, J.D. Sloppy, L. Guo, C.A. Grimes, Vertically aligned WO(3) nanowire arrays grown directly on transparent conducting oxide coated glass: synthesis and photoelectrochemical properties, Nano letters, 11 (2011) 203–208.

[7] G. Wang, Y. Ling, H. Wang, X. Yang, C. Wang, J.Z. Zhang, Y. Li, Hydrogen-treated WO3 nanoflakes show enhanced photostability, Energy & Environmental Science, 5 (2012) 6180–6187.

[8] L. Villaseca, B. Moreno, I. Lorite, J.R. Jurado, E. Chinarro, Synthesis and characterization of tungsten nitride (W2N) from WO3 and H2WO4 to be used in the electrode of electrochemical devices, Ceramics International, 41 (2015) 4282–4288.
[9] M. Radecka, P. Sobas, M. Wierzbicka, M. Rekas, Photoelectrochemical properties of undoped and Ti-doped WO3, Physica B: Condensed Matter, 364 (2005) 85-92.
[10] X.F. Cheng, W.H. Leng, D.P. Liu, J.Q. Zhang, C.N. Cao, Enhanced photoelectrocatalytic performance of Zn-doped WO(3) photocatalysts for nitrite ions degradation under visible light, Chemosphere, 68 (2007) 1976–1984.
[11] Z. Yan, M. Cai, P.K. Shen, Nanosized tungsten carbide synthesized by a novel route at low temperature for high performance electrocatalysis, Scientific reports, 3 (2013) 1646.
[12] C. Janáky, K. Rajeshwar, N.R. de Tacconi, W. Chanmanee, M.N. Huda, Tungsten-based oxide semiconductors for solar hydrogen generation, Catalysis Today, 199 (2013) 53–64.
[13] Y. Liu, Y. Li, W. Li, S. Han, C. Liu, Photoelectrochemical properties and photocatalytic activity of nitrogen-doped nanoporous WO3 photoelectrodes under visible light, Applied Surface Science, 258 (2012) 5038–5045.
[14] T. Takata, K. Domen, Development of non-oxide semiconductors as light harvesting materials in photocatalytic and photoelectrochemical water splitting, Dalton transactions, (2017).
[15] B. Cole, B. Marsen, E. Miller, Y. Yan, B. To, K. Jones, M. Al-Jassim, Evaluation of Nitrogen Doping of Tungsten Oxide for Photoelectrochemical Water Splitting, The Journal of Physical Chemistry C, 112 (2008) 5213–5220.
[16] M.R. Berber, I.H. Hafez, T. Fujigaya, N. Nakashima, A highly durable fuel cell electrocatalyst based on double-polymer-coated carbon nanotubes, Scientific reports, 5 (2015) 16711.
[17] P. Bai, W. Xing, Z. Yan, Synthesis and characterization of mesostructured tungsten nitride by using tungstic acid as the precursor, Journal of Porous Materials, 13 (2006) 173–180.
[18] Y.C. Nah, I. Paramasivam, R. Hahn, N.K. Shrestha, P. Schmuki, Nitrogen doping of nanoporous WO3 layers by NH3 treatment for increased visible light photoresponse, Nanotechnology, 21 (2010) 105704.
[19] M.D. Lyutaya, Formation of nitrides of the Group VI transition metals, Soviet Powder Metallurgy and Metal Ceramics, 18 (1979) 190–196.
[20] Q. Zhong, S.A. Wessel, B. Heinrich, K. Colbow, The electrochromic properties and mechanism of H3WO3 and LixWO3, Solar Energy Materials, 20 (1990) 289–296.

[21] F. Xu, A. Fahmi, Y. Zhao, Y. Xia, Y. Zhu, Patterned growth of tungsten oxide and tungsten oxynitride nanorods from Au-coated W foil, Nanoscale, 4 (2012) 7031–7037.
[22] S. Wang, X. Yu, Z. Lin, R. Zhang, D. He, J. Qin, J. Zhu, J. Han, L. Wang, H.-k. Mao, J. Zhang, Y. Zhao, Synthesis, Crystal Structure, and Elastic Properties of Novel Tungsten Nitrides, Chemistry of Materials, 24 (2012) 3023–3028.
[23] I.M. Szilágyi, J. Pfeifer, C. Balázsi, A.L. Tóth, K. Varga-Josepovits, J. Madarász, G. Pokol, Thermal stability of hexagonal tungsten trioxide in air, Journal of Thermal Analysis and Calorimetry, 94 (2008) 499–505.
[24] B. Weng, J. Wu, N. Zhang, Y.J. Xu, Observing the role of graphene in boosting the two-electron reduction of oxygen in graphene-WO(3) nanorod photocatalysts, Langmuir : the ACS journal of surfaces and colloids, 30 (2014) 5574–5584.
[25] I.M. Szilágyi, B. Fórizs, O. Rosseler, Á. Szegedi, P. Németh, P. Király, G. Tárkányi, B. Vajna, K. Varga-Josepovits, K. László, A.L. Tóth, P. Baranyai, M. Leskelä, WO3 photocatalysts: Influence of structure and composition, Journal of Catalysis, 294 (2012) 119–127.
[26] V. Chakrapani, J. Thangala, M.K. Sunkara, WO3 and W2N nanowire arrays for photoelectrochemical hydrogen production, International Journal of Hydrogen Energy, 34 (2009) 9050–9059.
[27] R.F. Garcia-Sanchez, T. Ahmido, D. Casimir, S. Baliga, P. Misra, Thermal effects associated with the Raman spectroscopy of WO3 gas-sensor materials, The journal of physical chemistry. A, 117 (2013) 13825–13831.
[28] D.K. Nandi, U.K. Sen, S. Sinha, A. Dhara, S. Mitra, S.K. Sarkar, Atomic layer deposited tungsten nitride thin films as a new lithium-ion battery anode, Physical Chemistry Chemical Physics, 17 (2015) 17445–17453.
[29] Y.G. Shen, Y.W. Mai, Effect of deposition conditions on internal stresses and microstructure of reactively sputtered tungsten nitride films, Surface and Coatings Technology, 127 (2000) 238–245.
[30] M. Nagai, T. Suda, K. Oshikawa, N. Hirano, S. Omi, CVD preparation of alumina-supported tungsten nitride and its activity for thiophene hydrodesulfurization, Catalysis Today, 50 (1999) 29–37.
[31] K. Nakagawa, N. Miura, S. Matsumoto, R. Nakano, H. Matsumoto, Electrochromism and Electronic Structures of Nitrogen Doped Tungsten Oxide Thin Films Prepared by RF Reactive Sputtering, Japanese Journal of Applied Physics, 47 (2008) 7230–7235.

[32] R. Asahi, T. Morikawa, T. Ohwaki, K. Aoki, Y. Taga, Visible-Light Photocatalysis in Nitrogen-Doped Titanium Oxides, Science, 293 (2001) 269–271.
[33] A. Watcharenwong, W. Chanmanee, N.R. de Tacconi, C.R. Chenthamarakshan, P. Kajitvichyanukul, K. Rajeshwar, Anodic growth of nanoporous WO3 films: Morphology, photoelectrochemical response and photocatalytic activity for methylene blue and hexavalent chrome conversion, Journal of Electroanalytical Chemistry, 612 (2008) 112–120.
[34] C. Janáky, W. Chanmanee, K. Rajeshwar, On the Substantially Improved Photoelectrochemical Properties of Nanoporous WO3 Through Surface Decoration with RuO2, Electrocatalysis, 4 (2013) 382–389.
[35] K. Gelderman, L. Lee, S.W. Donne, Flat-Band Potential of a Semiconductor: Using the Mott–Schottky Equation, Journal of Chemical Education, 84 (2007) 685–688.